CHARACTERISTICS OF A SUBCRITICAL ASSEMBLY EVALUATED BY NEUTRON WAVES

by

Frank Peter Mertes

A Thesis Submitted to the
Graduate Faculty in Partial Fulfillment of
The Requirements for the Degree of

MASTER OF SCIENCE

Major Subject: Nuclear Engineering

Iowa State University
Of Science and Technology
Ames, Iowa

1959

TABLE OF CONTENTS

I. INTRODUCTION

The neutron flux distribution within a system which has present a periodically varying source may be conveniently analyzed by use of the concept of neutron waves. With such a periodically varying source the time-dependent diffusion equation is used to describe the flux as a function of both time and space. The use of this procedure facilitates the determination of the nuclear parameters, specifically the diffusion length and the material buckling. The use of this method, which is analogous to Angestrom's cyclic method of measuring thermal conductivity, can be applied to both multiplying and non-multiplying media. In this investigation the complex material buckling in a graphite-uranium assembly was studied.

The complex material buckling in an assembly is dependent upon the frequency of the source, increasing with increasing frequency. With this increase in the complex material buckling, it is possible to obtain measurements in much smaller systems than are used for exponential experiments. On this basis the use of the neutron wave analysis should permit measurements of the material buckling in the existing subcritical assembly that would be comparable in accuracy to those obtained in larger systems. A new and more effective method of studying the phase angle and amplitude of the neutron waves in the subcritical assembly by a completely analytical method, with no dependence upon visual interpretation of graphs, has been developed.

The phase and amplitude of the neutron wave was determined as a function of vertical position in the assembly for two frequencies of

oscillation. Phase and amplitude determinations were also made along a horizontal plane in the assembly.

II. REVIEW OF THE LITERATURE

The existence of attenuated neutron waves within an assembly, which can be used rather effectively in the evaluation of nuclear parameters, can be brought about by a periodic disturbance of the system.

The theory has been developed to a large extent by Weinberg. An early paper by Weinberg and Schweinler (5) describes the neutron waves produced in a just critical reactor by the oscillation of a neutron absorber. It is stated that at frequencies which are low compared to the periods of the delayed neutrons, the neutron flux intensity in the reactor rises and falls as a whole, the shape of the stationary distribution always being maintained. As the frequency of the oscillation is increased, the nature of the neutron response changes from the overall fluctuation characteristic at low frequency to a propagated and attenuated spherical neutron wave which emanates from the vicinity of the oscillator. The amplitude of the oscillating response for a given frequency is proportional to the total neutron absorption crossection of the oscillated absorber. This technique has been used in the determination of absorption crossection.

Weinberg and Wigner (6) discuss the propagation of neutron waves in both multiplying and non-multiplying media. Their development in both cases is undertaken for the case of a periodically varying source in an infinite homogenous medium. Equations describing the neutron wave velocity, wave length, and attenuation length as functions of the nuclear parameters of the assembly and the frequency of oscillation are developed.

Experimental work on the neutron wave propagation in a

non-multiplying medium was carried out in France by Raievski and Horowitz (3). They determined the diffusion coefficient of heavy water using a periodically varying radioactive antimony source which was allowed to irradiate a beryllium block, thereby producing a periodic neutron source. By measurement of the neutron waves produced it was possible to determine the diffusion coefficient of heavy water quite accurately.

Campbell and Stelson (1) have used the pulsed source technique to study neutron waves in multiplying media. The relaxation time measurements were made of the decay of the fundamental mode of thermal neutron in several sizes of subcritical assemblies using U^{235} H_2O solutions. A square wave pulsed neutron source and a multichannel time analyser were used. The dependence of relaxation time on reactor size made possible the calculation of the multiplicative properties and characteristic nuclear parameters. Neutron bursts, generated by an accelerator with beryllium target, were used to excite uranyl fluoride solution in cylindrical containers. The neutrons leaking out between bursts were detected with a LiI scintillation counter. The half life of the emitted neutrons was measured for several different values of geometric buckling.

III. LIST OF SYMBOLS

a	Length of assembly	cm.
b	Width of assembly	cm.
c	Height of assembly	cm.
B^2	Buckling	$cm.^{-2}$
B_m^2	Static material buckling	$cm.^{-2}$
C_m	Count rate, mean value over interval	counts/min.
C_s	Count rate, corresponding to the steady state	counts/min.
C_w	Count rate corresponding to the amplitude of the wave -	counts/min.
D	Thermal neutron diffusion coefficient	cm.
k_ρ	Infinite multiplication factor	
L_a	Attenuation length	cm.
L_w	Wave length	cm.
R	Time for one revolution of oscillator drum	sec.
S	Neutron source strength	$neutrons/cm.^3$-sec.
t	Time	sec.
v	Thermal neutron velocity	cm./sec.
V	Propagation velocity of neutron wave	cm./sec.
β_M^2	Complex material buckling	$cm.^{-2}$
γ	Inverse relaxation length	$cm.^{-1}$
θ	Phase angle of the neutron wave	radians
Σ_a	Thermal neutron absorption crossection	$cm.^2$
Φ	Space dependent thermal neutron flux	$neutrons/cm.^2$-sec.
φ	Thermal neutron flux	$neutrons/cm.^2$-sec.
ω	Angular frequency	radians/sec.

IV. THEORETICAL ANALYSIS

The analyses of the neutron wave propagation in non-multiplying and subcritical assemblies have been developed by Uhrig.* The relationships for the non-multiplying medium will be considered first.

The neutrons are emitted from a periodically varying source located at the bottom of a parallelepiped of diffusing and moderating material. The varying source will be expressed by $S + S\, e^{i\,t}$. The homogeneity of the medium refers to the fact that the diffusion coefficient, macroscopic absorption crossection, and thermal neutron velocities are the same throughout the assembly.

If an arbitrary cubic centimeter of the assembly is chosen, a thermal neutron balance equation may be written.

$$(1)\quad \frac{1}{v}\frac{\partial \varphi}{\partial t}(r,t) = D\nabla^2\varphi(r,t) - \Sigma a\ \varphi(r,t) + S$$

In the above equation $D\nabla^2\varphi(r,t)$ represents the net diffusion into the selected volume element, $\Sigma a\ \varphi(r,t)$ represents the absorption by the diffusing medium and S represents the neutrons supplied by thermalization within the volume element, and $\frac{1}{v}\frac{\partial \varphi}{\partial t}(r,t)$ represents the time rate of change of neutron density.

The thermal neutron flux throughout the volume will have the same time dependence as the source.

$$(2)\quad \varphi(r,t) + \bar{\Phi}_0(r) + \bar{\Phi}(r)\, e^{i\omega t}$$

implying that the variables of time and space are separable.

---

*Uhrig, R. E., Ames, Iowa. Neutron wave propagation. Private communication. May, 1959.

Outside the region where the neutrons are becoming thermalized by moderation, that is, at distances far from the source, S = 0 and Eq. (1) may be written as

$$(3)\quad \frac{i\omega}{v}\Phi(r)e^{i\omega t} = D\nabla^2[\Phi_0(r) + \Phi(r)e^{i\omega t}] - \Sigma_a \Phi_0(r)e^{i\omega t}$$

For the steady component of the flux, Eq. (1) becomes

$$(4)\quad D\nabla^2 \Phi_0(r) - \Sigma_a \Phi_0(r) = 0$$

and substitution of Eq. (4) into Eq. (3) will eliminate the steady component of the neutron flux. This means that the steady and sinusoidal components of the neutron flux are separable. After division by $De^{i\omega t}$ Eq. (3) becomes,

$$(5)\quad \nabla^2 \Phi(r) - \gamma^2 \Phi(r) = 0$$

where

$$(6)\quad \gamma^2 = \frac{\Sigma_a}{D} + \frac{i\omega}{Dv} = \mu^2 + \frac{i\omega}{Dv}$$

Since the source is located at the bottom of a rectangular parallelepiped Eq. (5) can be most conveniently written using rectangular coordinates.

$$(7)\quad \frac{\partial^2 \Phi}{\partial x^2} + \frac{\partial^2 \Phi}{\partial y^2} + \frac{\partial^2 \Phi}{\partial z^2} - \gamma^2 = 0$$

If it is assumed that the flux is described as a product of three

terms each of which is a function of only one variable,

$$(8)\quad \Phi(x,y,z) = X(x)\,Y(y)\,Z(z)$$

Substitution of Eq. (8) into Eq. (7) and division by $(x\,y\,x)$ gives

$$(9)\quad \frac{X''}{X} + \frac{Y''}{Y} + \frac{Z''}{Z} - M^2 = 0$$

Since each of the terms in Eq. (9) is a function of one variable only the variables x, y and z are separable, and Eq. (9) can be true only if each of the terms is a constant. When the first three terms of Eq. (9) are replaced by constants $-\alpha_1^2 - \beta^2$ and $+\gamma^2$ Eq. (8) becomes

$$(10)\quad -\alpha^2 - \beta^2 + \gamma^2 - M^2 = 0$$

$$(11)\quad \frac{d^2X}{dx^2} + \alpha^2 X = 0$$

$$(12)\quad \frac{d^2Y}{dy^2} + \beta^2 Y = 0$$

$$(13)\quad \frac{d^2Z}{dz^2} + \gamma^2 Z = 0$$

The differential Eq. (11), (12) and (13) are readily solved to yield

$$(14)\quad X = C_1 \cos \alpha x + C_2 \sin \alpha x$$

$$(15)\quad Y = C_3 \cos \beta y + C_4 \sin \beta y$$

$$(16)\quad Z = C_5 e^{-\gamma z} - C_6 e^{+\gamma z}$$

These equations are subject to the following boundary conditions

$$(17)\quad \Phi\left(\pm\frac{a}{2}, y, z\right) = 0$$

$$(18)\quad \Phi\left(x, \pm\frac{b}{2}, z\right) = 0$$

$$(19)\quad \Phi(x, y, c) = 0$$

When the boundary conditions are applied to Eq. (14), (15) and (16) and the trivial solution that the flux is zero everywhere is discarded, Eq. (14), (15) and (16) become

$$(20)\quad X = C_1 \cos\frac{m\pi x}{a}$$

$$(21)\quad Y = C_3 \cos\frac{n\pi y}{b}$$

$$(22)\quad Z = C_5 e^{-\gamma z}\left[1 - e^{-2\gamma(c-z)}\right]$$

where m and n are odd integers.

When the flux is measured at a reasonable distance from the top of the assembly the end correction factor, the expression within the brackets of Eq. (22), is approximately equal to unity. Since the flux is not measured near the top of the assembly the end correction term will be considered to be equal to unity. There are an infinite number of odd integer values for m and n which give solutions of the form of Eq. (20) and (21). The general solution is a linear combination of all the possible solutions. Therefore Eq. (10) indicates that there is also an infinite number of values for mn. Upon substitution of Eq. (14), (15) and (16) into Eq. (8),

$$(23)\quad \Phi(x, y, z) = \sum_{m\,n} C_{mn} \cos\frac{m\pi x}{a} \cos\frac{n\pi y}{b}\, e^{-\gamma_{mn} z}$$

where all constants have been combined into a single generalized constant $C_{m,n}$

When the flux is assumed to be equal to the infinite summation of individual solutions to Eq. (20) and (21), a Fourier cosine series is obtained. It can be shown that the coefficients of the terms higher than the first become insignificant at a short distance from the bottom of the assembly. The flux can then be approximated quite well by the following equation, which contains only the first term of an infinite series of terms.

$$(24)\quad \Phi(x, y, z) = C \cos \frac{\pi x}{a} \cos \frac{\pi y}{b} e^{-\gamma z}$$

When Eq. (10) is rewritten using m = n = 1, it becomes,

$$(25)\quad \gamma^2 = M^2 + \left(\frac{\pi}{a}\right)^2 + \left(\frac{\pi}{b}\right)^2$$

or upon substitution of Eq. (6)

$$(26)\quad \gamma^2 = \mu^2 + \frac{i\omega}{Dv} + \left(\frac{\pi}{a}\right)^2 + \left(\frac{\pi}{b}\right)^2 = \nu^2 + \frac{i\omega}{Dv}$$

where

$$(27)\quad \nu^2 = \mu^2 + \left(\frac{\pi}{a}\right)^2 + \left(\frac{\pi}{b}\right)^2$$

It should be pointed out that ν^2 is the inverse relaxation length of the neutron flux in the z direction when a steady neutron source is used beneath the graphite assembly.

The complex root of Eq. (26) is

$$(28)\quad \gamma = \left(\frac{\nu^2}{2} + \rho^2\right)^{\frac{1}{2}} + i\left(\frac{\rho^2 - \nu^2}{2}\right)^{\frac{1}{2}}$$

where

$$(29)\quad \rho^2 = \left[\nu^4 + \left(\frac{\omega}{Dv}\right)^2\right]^{\frac{1}{2}}$$

The solution of the diffusion Eq. (5) for the steady state component of the neutron flux Φ_o using the boundary conditions and assumptions as above is given by Glasstone and Edlund to be

$$(30)\quad \Phi_o(r) = C_o \cos\frac{\pi x}{a} \cos\frac{\pi y}{b}\, e^{-\nu z}$$

Eq. (24) and (30) are substituted into Eq. (2) to give

$$(31)\quad \varphi(x, y, z, t) = C_o \cos\frac{\pi x}{a} \cos\frac{\pi y}{b}\, e^{-\nu z} + C \cos\frac{\pi x}{a} \cos\frac{\pi y}{b}\, e^{-\gamma z}\, e^{i\omega t}$$

Substitution of Eq. (28) into Eq. (31) and grouping of imaginary terms gives

$$(32)\quad \varphi(x, y, z, t) = C_o \cos\frac{\pi x}{a} \cos\frac{\pi y}{b}\, e^{-\nu z} + C \cos\frac{\pi x}{a} \cos\frac{\pi y}{b}\, e^{-\left(\frac{\nu^2 + \rho^2}{2}\right)^{\frac{1}{2}} z} e^{i\left[\omega t - \left(\frac{\rho^2}{2} - \nu^2\right)^{\frac{1}{2}} z\right]}$$

The imaginary exponent of the last term in Eq. (32) can be written in the form $i\omega(t - T)$ where T is the time necessary for the neutron wave to travel from the source to the level z.

$$(33)\quad T = \left(\frac{\rho^2 - \nu^2}{2}\right)^{\frac{1}{2}} \frac{z}{\omega} = \frac{z}{Vw}$$

where Vw is the velocity of the neutron wave.

From Eq. (32) and (33) the following properties of the neutron wave are readily apparent:

Attenuation length of the neutron wave amplitude is

$$(34)\quad L_a = \left(\frac{2}{\nu^2 + \rho^2}\right)^{\frac{1}{2}}$$

Velocity of neutron wave propagation is

$$(35)\quad V_w = \omega\left(\frac{2}{\rho^2 - \nu^2}\right)^{\frac{1}{2}}$$

Wave length of the neutron wave is

$$(36)\quad L_w = 2\pi\left(\frac{2}{\rho^2 - \nu^2}\right)^{\frac{1}{2}}$$

In the case of the neutron wave propagation through a multiplying medium the formal analysis is essentially the same as that just completed. Once again the medium will be assumed to be homogeneous. While the graphite-uranium lattice is obviously heterogeneous, the lattice pattern is repeated and uniform and can be homogenized to give the overall flux distribution.

The time rate of change of the thermal neutron population is equal to

$$(37)\quad \frac{1}{v}\frac{\partial \varphi(r,t)}{\partial t} = D\nabla^2\varphi(r,t) - \Sigma a\,\varphi(r,t) + S$$

The source term is composed of two contributions; the thermal neutron population is increased by the thermalization of neutrons from both the external sources S_{EXT} and from fission S_f. The fission source is given

by Glasstone and Edlund to be

$$(38)\quad S_f = k_p \Sigma a \; e^{-\beta^2 \tau}$$

The contribution of the external source is zero except near the bottom of the assembly. The prompt multiplication factor is used since the period of the oscillation is short compared to delayed neutron lifetimes, and the delayed neutrons add slightly to the steady component of the flux. The thermal neutron flux throughout the assembly will again have the form

$$(39)\quad \varphi(r,t) = \Phi_0(r) + \Phi(r)\, e^{i\omega t}$$

Substitution of Eq. (38) and (39) into Eq. (37) and elimination of the steady component of neutron flux in a manner similar to that previously used gives

$$(40)\quad \nabla^2 \varphi(r,t) + \beta_M^2 \varphi(r,t) = 0$$

where β_M^2, the complex material buckling is given by,

$$(41)\quad \beta_M^2 = \frac{\Sigma a}{D} k_p (e^{-\beta^2 \tau} - 1) - \frac{i\omega}{vD} = B_M^2 - \frac{i\omega}{vD}$$

Eq. 40 can be solved in rectangular coordinates subject to the same boundary conditions as in the case of the non-multiplying medium to give

$$(42)\quad \varphi(x, y, z, t) = C_0 \cos \frac{\pi x}{a} \cos \frac{\pi y}{b}\, e^{-\lambda z} + C \cos \frac{\pi x}{a} \cos \frac{\pi y}{b}\, e^{-\gamma z}\, e^{i\omega t}$$

where

$$(43)\quad \gamma^2 = \left(\frac{\pi}{a}\right)^2 + \left(\frac{\pi}{b}\right)^2 - \beta_M^2 = \left(\frac{\pi}{a}\right)^2 + \left(\frac{\pi}{b}\right)^2 - B_M^2 + \frac{i\omega}{Dv}$$

and by definition

$$(44)\quad \Lambda^2 = \left(\frac{\pi}{a}\right)^2 + \left(\frac{\pi}{b}\right)^2 - B_M^2$$

Here again Λ is the inverse relaxation length of the neutron flux in the z direction when a steady neutron source is used beneath the subcritical assembly. Substitution of Eq. (44) into Eq. (43) gives

$$(45)\quad \gamma^2 = \Lambda^2 + \frac{i\omega}{vD}$$

The complex root of Eq. (45) is

$$(46)\quad \gamma = \pm\left(\frac{\Lambda^2 + \Psi^2}{2}\right)^{\frac{1}{2}} + i\left(\frac{\Psi^2 - \Lambda^2}{2}\right)^{\frac{1}{2}}$$

where

$$(47)\quad \Psi^2 = \left[\Lambda^4 + \left(\frac{\omega}{Dv}\right)^2\right]^{\frac{1}{2}}$$

When Eq. (46) is substituted into Eq. (42),

$$(48)\quad \varphi(x,y,z,t) = C_o \cos\frac{\pi x}{a}\cos\frac{\pi y}{b}\, e^{-\Lambda z}$$

$$+ C \cos\frac{\pi x}{a}\cos\frac{\pi y}{b}\, e^{-\left(\frac{\Lambda^2+\Psi^2}{2}\right)^{\frac{1}{2}} z}\, e^{i\left[\omega t - \left(\frac{\Psi^2-\Lambda^2}{2}\right)^{\frac{1}{2}} z\right]}$$

Again it is readily apparent that the following relationships hold:

Attenuation length of the amplitude of the neutron wave is

(49) $L_a = \left(\frac{2}{\Lambda^2 + \psi^2}\right)^{\frac{1}{2}}$

Propagation velocity of the neutron wave is

(50) $V_w = \left(\frac{2}{\psi^2 - \Lambda^2}\right)^{\frac{1}{2}}$

Wave length of the neutron wave is

(51) $L_w = 2\pi \left(\frac{2}{\psi^2 - \Lambda^2}\right)^{\frac{1}{2}}$

V. EXPERIMENTAL EQUIPMENT

A. Subcritical Assembly

The subcritical assembly employed in this investigation was composed of natural uranium and graphite. The blocks of graphite were of AGR grade, and had been machined from a 7 inch diameter rod to a 6 inch by 6 inch square. These blocks composed the bottom 9 rows of the assembly, while the top 5 rows were machined to a 5 inch by 6 inch rectangle from a 6-3/8 inch diameter rod. The graphite rods rested upon a wooden support, under which the thermal neutron sources were placed.

The natural uranium was present in the form of 1 inch diameter slugs encased in 2S aluminum cans. The canned slugs were placed in horizontal aluminum tubes, 62 inches long which had an outside diameter of 1.375 inches, and a wall thickness of 0.035 inches. Aluminum wire wound in a spiral centered the canned slugs in the aluminum tubes. The tubes each containing 7 slugs were arranged to form an 8½ inch lattice within the graphite moderator.

The extrapolated dimensions of the subcritical assembly a, b, and c were 62.0, 64.0, and 79.8 inches respectively. With the 8½ inch lattice employed the static material buckling was $51.6 \pm 11.9 \times 10^{-6}$ cm.$^{-2}$

B. Oscillator Unit

The oscillator unit, which is shown in Fig. 1, contained 5 one-curie Pu-Be neutron sources. The neutrons were moderated by a 3-inch layer of

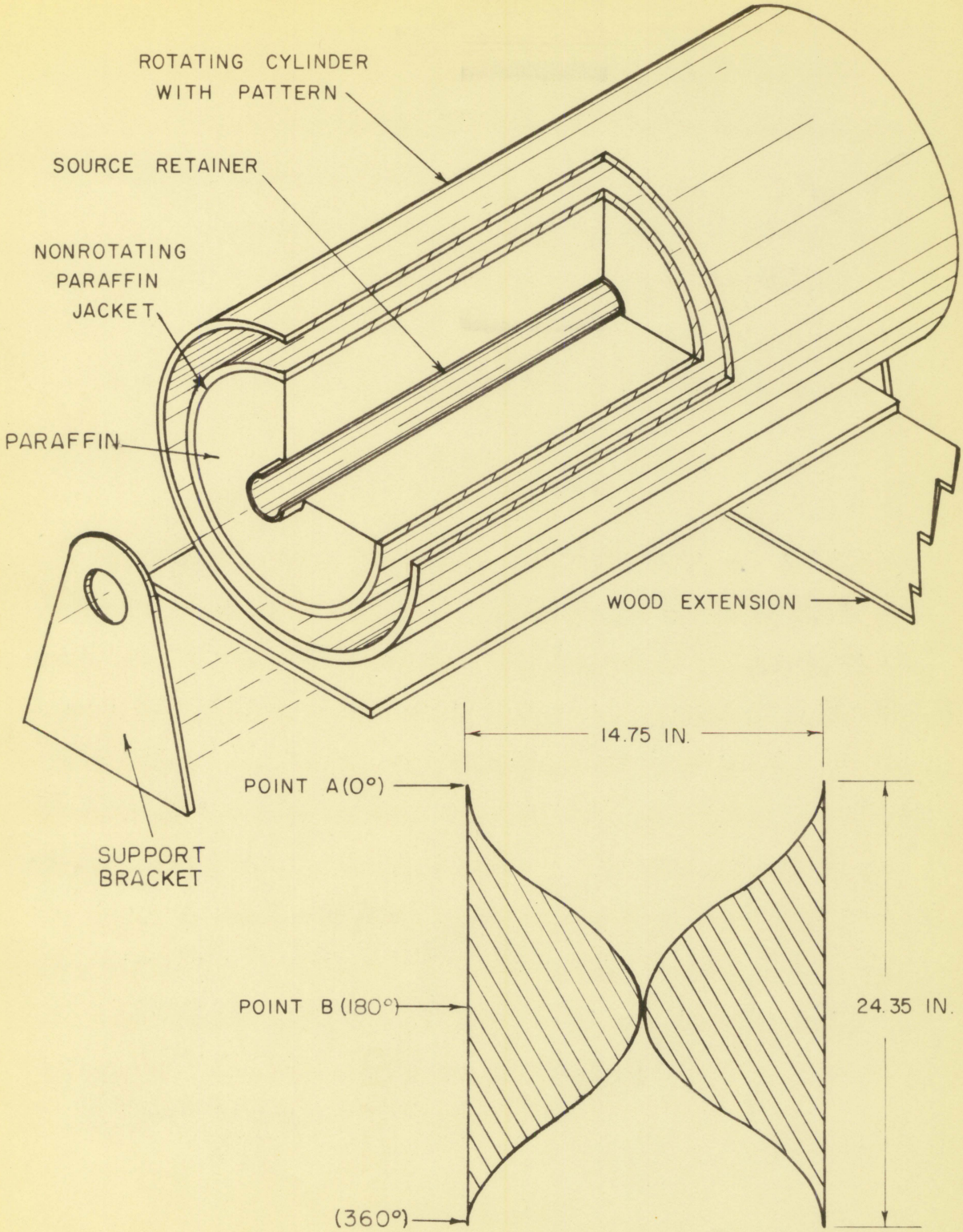
ROTATING CYLINDER
WITH PATTERN
SOURCE RETAINER
NONROTATING
PARAFFIN
JACKET
PARAFFIN
WOOD EXTENSION
SUPPORT
BRACKET
14.75 IN.
POINT A(0°)
POINT B(180°)
(360°)
24.35 IN.

paraffin, and hence a large percentage of the neutrons were thermalized by the time they reached the outer surface of the drum. An outer rotating cylinder, the pattern cylinder, was constructed of aluminum, with a neutron absorbing pattern of cadmium cemented on the inside surface. This pattern, cut in the form of a sine wave as shown in Fig. 1, was 0.030 inches thick. As the pattern cylinder rotated it changed the rate at which the neutrons were emitted from the source, causing the neutron flux intensity to vary in a sinusoidal manner.

C. Drive Mechanism

In order to measure the neutron wave propagation, it was necessary to determine the exact amount of rotation of the oscillator drum. A chain drive was used to synchronize the rotation of the oscillator drum beneath the assembly and the rotation indicator placed beyond the edge of the assembly. The rotation indicator consisted of a countershaft with a sprocket for the chain drive to the drum, a pulley leading to the drive motor, a disc fixed to the shaft and calibrated to correspond to the oscillator drum rotation, and a light chopper which interrupted a light beam leading to a photocell. This chopper could be aligned with the calibrated disc to allow the light to fall on the photocell during any selected portion of the oscillator drum rotation.

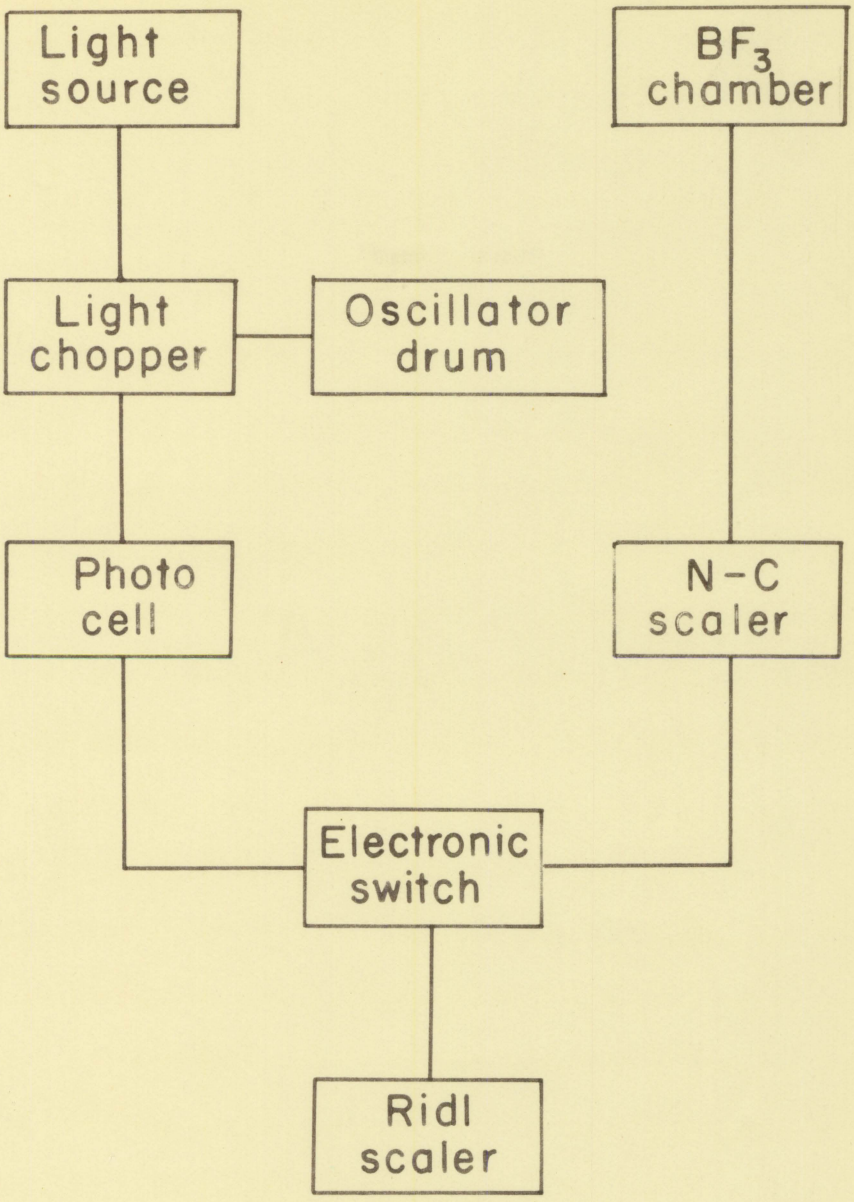

Fig. 2. Instrument arrangement

D. Electronic Equipment

The neutron flux was measured using a N. Wood, BF_3 neutron proportional counter. The chamber was filled with BF_3 at 40 mm of Hg, having an active volume of 28 cm^3 and a voltage plateau at 2400 volts. The pulses from the detector were fed into a Nuclear-Chicago Ultramatic scaler with the sensitivity set at 1 millivolt during the investigation. The Nuclear-Chicago scaler registered the total number of pulses produced in the BF_3 chamber, and these could be read off the conventional dials of the instrument. This scaler had a ratemeter jack on the rear of the chassis which gave an eight-volt pulse, approximately 3 microseconds wide, for each pulse produced in the BF_3 counter. As can be seen from the block diagram in Fig. 2, these pulses from the rate meter jack of the Nuclear-Chicago scaler were fed to an electronic switching circuit controlled by a photocell and thence to a second scaler. The second counter registered only those pulses which were produced in the BF_3 detector during those periods when the photocell was illuminated.

The light source was constructed from a conventional 2 cell lantern type flashlight wired to operate using alternating current supplied at 1.35 volts ac from a potentiometer across the output of a 6.3 volt ac power supply. Maintenance of a steady voltage to the light source was necessary to insure reproducibility of the data.

The beam from the light source was interrupted by a wooden chopper attached to the rotation indicator on the countershaft. The chopper could permit the photocell to be illuminated during any selected 180 degrees of rotation by means of its movement relative to the calibrated disc on the

rotation indicator. In this investigation only a 180 degree segment was used; any other desired interval could be selected by fabricating a new chopper.

The photocell was a 929 tube powered by a 90 volt B battery, since the current drain was very small during the normal operation. A photocell mask was devised to prevent extraneous light from influencing the proper operation of the photocell.

The output from both the photocell and the Nuclear-Chicago Ultramatic scaler were fed to the electronic switching circuit in which a 12Ax7 tube was utilized in a coincidence circuit. The tube was normally conducting when there was no signal at either the ratemeter jack or the photocell input. If either of these registered a signal, the associated grid went negative, stopping current flow in one half of the tube. However, the other half of the tube accommodated the majority of the load change and only a small pulse was registered at the output. If both grids went negative at the same time; that is, a pulse came through from the scaler when the photocell was illuminated, practically all current flow stopped and a large pulse was registered at the output. Figure 3 contains a circuit diagram of the system described above.

The output pulses from the electronic switching circuit were fed to a RIDL-206 scaler. By adjusting the pulse height selector on this instrument, it was possible to discriminate against the smaller pulses caused by only one grid going negative and count the larger pulses brought about by both grids being driven negative at the same time. Thus this second

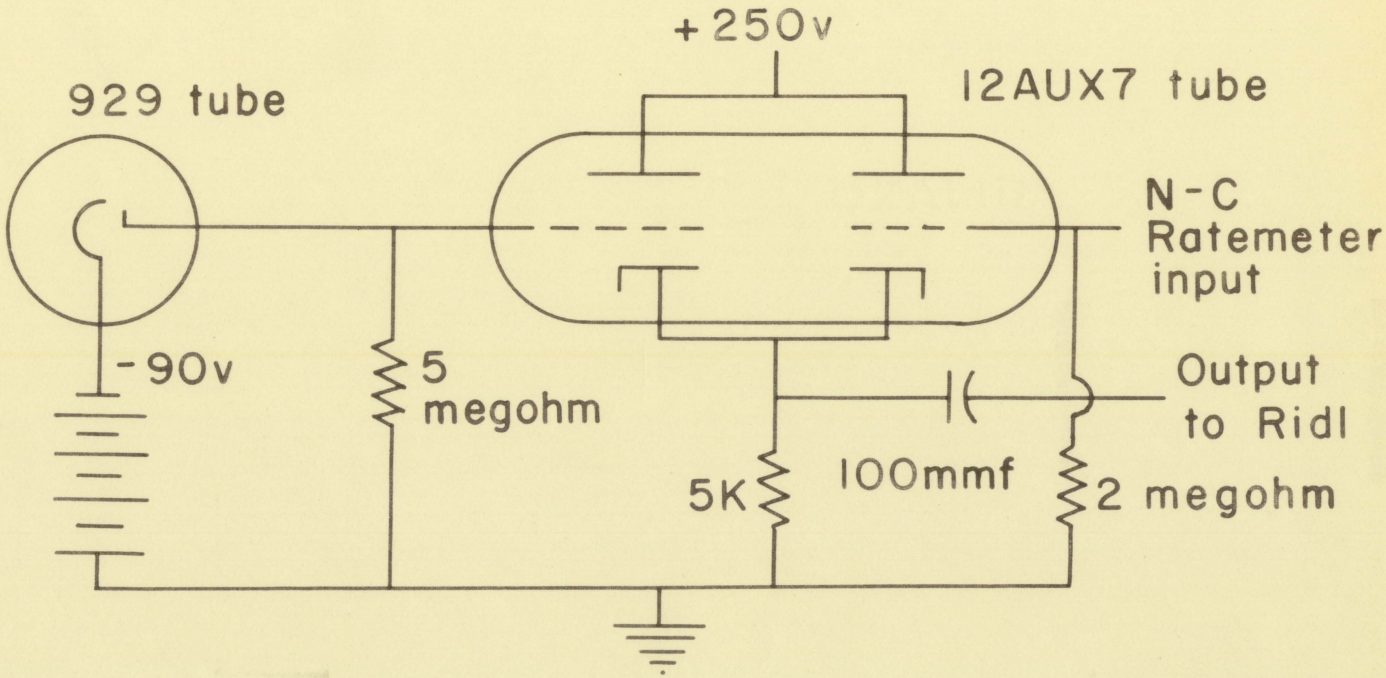

Fig. 3. Circuit diagram of electronic switch

counter registered those counts which occurred while the photocell was illuminated. Using this equipment, the time lag of mechanical switches was eliminated, and a large amount of flexibility was incorporated into the equipment.

VI. EXPERIMENTAL PROCEDURE

A. Analysis of Neutron Waves

The primary concern in the development of experimental techniques was the need to obtain a means of evaluating directly the phase and amplitude of the neutron waves.

When these quantities are known, the velocity of propagation and the attenuation of the neutron wave at various positions within the subcritical assembly could be studied. In a first attempt to study the neutron waves directly, the output from a BF_3 probe was fed to an electrometer and subsequently to a recording potentiometer. Unfortunately the electrical currents produced by the BF_3 chamber were quite low, about 10^{-13} amperes. While such small currents could be measured with the electrometer, a long period was required for the instrument to reach an equilibrium reading. The delay was attributed to the large capacitance in the circuit, making it impossible to study the dynamic behavior of the neutron flux with this system.

An attempt to analyze the neutron waves by measurement of the amplitude of many individual segments of the waves and sketching of a composite curve was ruled out due to high statistical scatter produced by the very short effective counting interval. The method also involved a subjective interpretation of the points when sketching the sine curve.

A direct analytical approach was developed and is presented below. This analysis indicates the phase and amplitude of the attenuated neutron

wave at any point in the assembly. Only two measurements of neutron flux are required at that point.

In Fig. 4, the neutron count rate is plotted at some arbitrary point within the assembly, where the neutron wave lags the oscillator source by a phase angle θ. The count rate at this point can be written as a function of time.

$$(52)\quad C = C_w \sin\left(\frac{2\pi t}{R} - \theta\right) + C_S$$

$$(53)\quad C = C_w \left[\sin\frac{2\pi t}{R}\cos\theta - \cos\frac{2\pi t}{R}\sin\theta\right] + C_S$$

Since the BF_3 detector can measure neutron flux only during a finite time interval, the counter necessarily registers a total count during the interval from which a mean value count rate can be calculated. If an interval from $t = R/4$ to $t = 3R/4$ is designated as Interval 1, the mean value of the count rate in Interval 1 is given by the mean value theorem,

$$(54)\quad C_{M_1} = \frac{\displaystyle\int_{R/4}^{3R/4} C_w \cos\theta \sin\frac{2\pi t}{R} - \cos\frac{2\pi t}{R}\sin\theta\, dt + \int_{R/4}^{3R/4} C_{S_1}\, dt}{\displaystyle\int_{R/4}^{3R/4} dt}$$

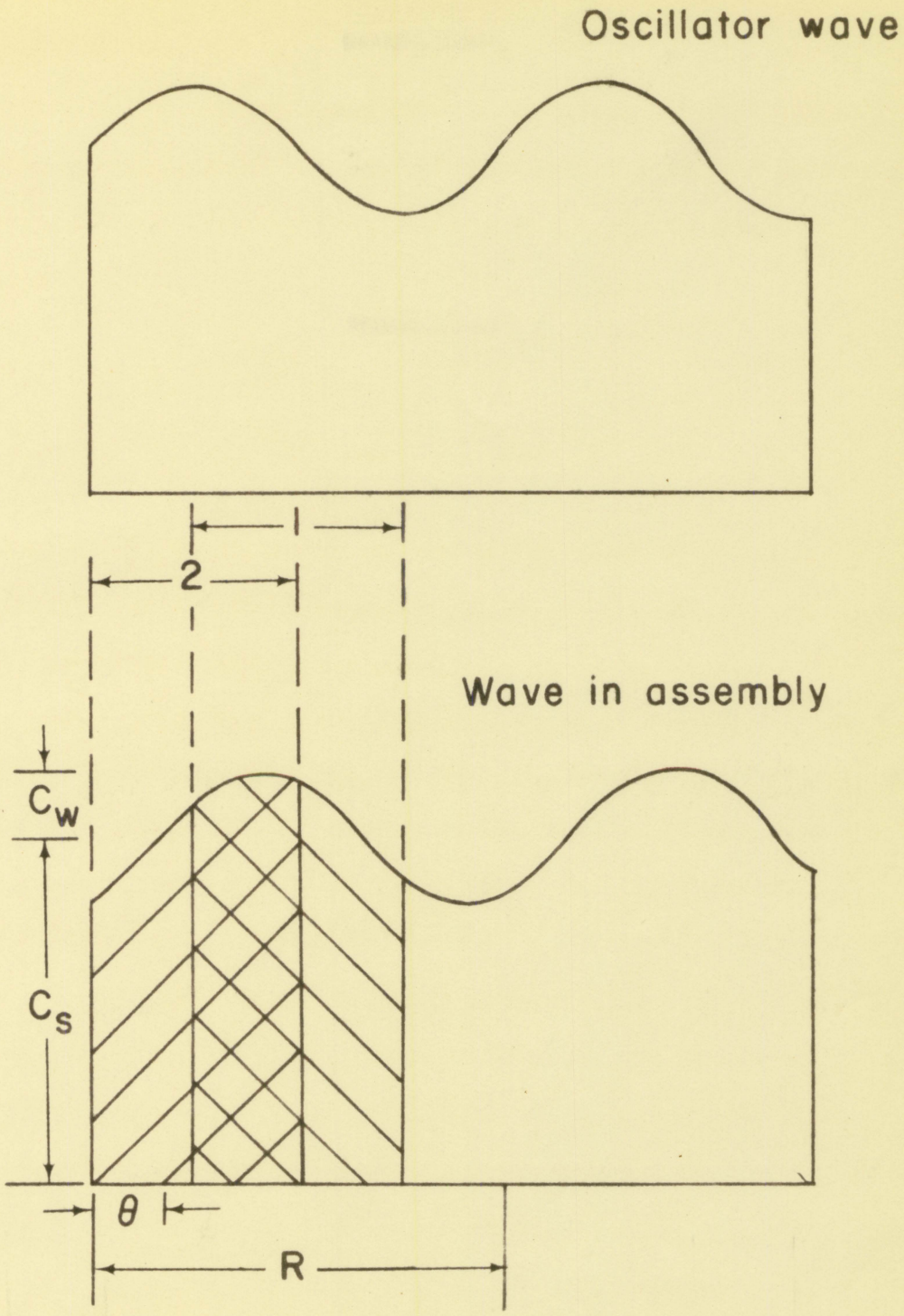

Fig. 4. Phase shift of neutron wave in assembly

When the above equation is integrated,

$$(55)\quad C_{M_1} - C_{S_1} = \frac{2C_W}{\pi} \sin\theta$$

Similarly Eq. (54) can be evaluated to give a mean value over Interval 2, for t = 0 to t = R/2.

$$(56)\quad C_{M_2} - C_{S_2} = \frac{2C_W}{\pi} \cos\theta$$

If Eq. (55) is divided by Eq. (56)

$$(57)\quad \tan\theta = \frac{C_{M_1} - C_{S_1}}{C_{M_2} - C_{S_2}}$$

When Eq. 56 is solved for C_W

$$(58)\quad C_W = \frac{\pi}{2} \frac{C_{M_1} - C_{S_1}}{\sin\theta}$$

Eq. (58) indicates that the amplitude can be determined only if the phase angle is known, actually the two equations are written with the two unknowns and C_W and it is possible to solve for each directly. The direct solution for C_W is however mathematically much more tedious.

Eq. (57) and Eq. (58) can be used to compute the amplitude and the phase shift directly from the readings of the two scalers employed. The mean values C_{M_1} and C_{M_2} are the count rates given by the RIDL scaler over the interval measured. The steady state readings C_{S_1} and C_{S_2} are the count rates indicated by the Nuclear Chicago scaler, since the steady state value is equal to the mean value over a time interval equal to R. In computing the mean count rates from the counts registered on the RIDL scalers, it must be noted that the RIDL scaler is counting only during

one half of the run.

By this simple method phase and amplitude determinations were made at various points in the assembly. The method is completely analytic and subject to analysis from the point of statistical validity of the data obtained. Since the RIDL scaler registers counts during one-half of the time interval measured, a very high effective counting period was obtained, relative to approaches that registered counts only during small intervals of the revolution of the oscillator. This permitted high counts to be obtained in reasonable lengths of time.

An analysis of precision of the data is necessitated by the large statistical scatter noted. This analysis of both and C_w is based on generalized formula for the standard deviation as given by Worthington and Geffner (7).

$$(59)\quad \sigma_U^2 = \left(\frac{\partial U}{\partial x_1}\right)^2 \sigma_x^2 + \left(\frac{\partial U}{\partial x_2}\right)^2 \sigma_{x_2}^2 + \left(\frac{\partial U}{\partial x_3}\right)^2 \sigma_{x_3}^2 + \cdots\cdots$$

where U is a function of x_1, x_2, x_3 . . . . . .

If this generalized relationship is applied to Eq. 57 the standard deviation is expressed as,

$$(60)\quad \sigma_\theta^2 = \left(\frac{\partial \theta}{\partial C_{M_1}}\right)^2 \sigma_{C_{M_1}}^2 - \left(\frac{\partial \theta}{\partial C_{S_1}}\right)^2 \sigma_{C_{S_1}}^2 + \left(\frac{\partial \theta}{C_{M_2}}\right)^2 \sigma_{C_{M_2}}^2 + \left(\frac{\partial \theta}{\partial C_{S_2}}\right)^2 \sigma_{C_{S_2}}^2$$

The partial derivatives are then evaluated:

$$(61)\quad \frac{\partial \theta}{\partial C_{M_1}} = \frac{-1}{(1 + \tan^2 \theta)\,(C_{S_2} - C_{M_2})}$$

$$(62)\quad \frac{\partial \theta}{\partial C_{S_1}} = \frac{1}{(1 + \tan^2\theta)(C_{S_2} - C_{M_2})}$$

$$(63)\quad \frac{\partial \theta}{\partial C_{M_2}} = \frac{-(C_{M_1} - C_{S_1})}{(1 + \tan^2\theta)(C_{S_2} - C_{M_2})^2}$$

$$(64)\quad \frac{\partial \theta}{\partial C_{S_2}} = \frac{(C_{M_2} - C_{S_1})}{(1 + \tan^2\theta)(C_{S_2} - C_{M_2})^2}$$

When Eq. (61), (62), (63) and (64) are substituted into Eq. (60)

$$(65)\quad \sigma_\theta^2 = \frac{1}{1 + \tan^2} \left[\frac{\sigma^2 C_{M_1} + \sigma^2 C_{S_1}}{(C_{S_2} - C_{M_2})^2} + \frac{(C_{M_1} - C_{S_1})^2 (\sigma^2 C_{M_2} + \sigma^2 C_{S_2})}{(C_{S_2} - C_{M_2})^4} \right]$$

By a similar procedure the standard deviation may be found for the quantity C_w which is proportional to the amplitude of the neutron wave. If Eq. (59) is applied to Eq. (59), the standard deviation of C_w can be found.

$$(66)\quad \sigma_{C_w}^2 = \left(\frac{\partial C_w}{\partial C_{M_1}}\right)^2 \sigma_{C_{M_1}}^2 + \left(\frac{\partial C_w}{\partial C_{S_1}}\right)^2 \sigma_{C_{S_1}}^2 + \left(\frac{\partial C_w}{\partial \theta}\right)^2 \sigma_\theta^2$$

The partial derivatives are evaluated as follows:

$$(67)\quad \frac{\partial C_w}{\partial C_{M_1}} = -\frac{\pi}{2 \sin}$$

$$(68)\quad \frac{\partial C_w}{\partial C_{S_1}} = \frac{\pi}{2 \sin}$$

$$(69)\quad \frac{\partial C_w}{\partial \theta} = \frac{\pi (C_{M_1} - C_{S_1})(\cos\theta)}{2 \sin^2\theta}$$

When Eq. (67), (68), and (69) are substituted into Eq. (66) the result is

$$(70)\quad \sigma_{c_w}^2 = \frac{\pi^2}{4 \sin^2\theta}\left[\sigma_{C_{S_1}}^2 + \sigma_{C_{M_1}}^2 + \frac{(C_{M_1} - C_{S_1})^2}{\tan^2\theta}\,\sigma_\theta^2\right]$$

B. A Typical Run

In all cases difficulties were encountered due to the fact that C_W was very much less than C_S, tending to obscure phase changes in the waves. In an effort to remedy the situation longer counts resulting in more precise measurements were taken. As the point of neutron flux measurement is moved away from the source, the absolute count rate decreases. It was possible to obtain results of approximately equal precision at all levels by doubling the counting time for every one foot increase in distance from the source.

The first step in undertaking a typical run was to adjust the speed of rotation of the oscillator drum. The variation in speed was made possible by the use of a series wound drive motor with the supply voltage controlled by a variable transformer. Speed measurements were taken with a revolution counter using a one-minute run. An arbitrary maximum speed of rotation was set at 380 r.p.m., since the chain drive vibrated excessively at higher speeds. Speed of revolution was checked during the run and adjusted if it was found necessary. In general the speed regulation was quite satisfactory; the motor held the oscillator drum to within

2 r.p.m. of the desired speed for long periods without adjustment.

Once the speed had been properly adjusted it was necessary to position the discriminator on the RIDL scaler so that the small pulses generated by the electronic switch when the light beam was blocked by the chopper did not trigger the scaler, while the larger pulses generated when the light beam reached the photocell did trigger the second scaler. Two runs were taken as a check, the first counting the pulses during the interval from 0 to R/2, and the second counting the pulses from R/2 to R. The check required that the sum of these counts be equal to one-half of the total counts registered on the Nuclear-Chicago scaler.

With the discriminator and the speed of revolution properly adjusted, a 15 minute run over the interval desired was taken in Channel 1. This served as a reference run for the series. A 15 minute run was next made over this same interval in Channel 2, following which a 5 minute check was made against the reference run using Channel 1. If the results did not agree with the reference run the discriminator had to be reset and the data for that particular 15 minute run discarded. The series was continued in this fashion, taking one-15 minute run in Channel 1, two-15 minute runs in Channel 2, 4 runs in Channel 3, and 8 in Channel 4. This procedure succeeded in giving results which had approximately equal precision for all channels, since the count rates in the upper channels were lower. No runs were made in Channel 5 where the count rate was judged too low to yield significant data.

The series of runs were made for one speed and one selected interval of rotation. Next a series of runs were made at the same speed of rotation

but with the chopper displaced by 90 degrees to give counts over the second selected interval. From these two series of runs the phase shift and amplitude attenuation in the vertical direction could be calculated.

Two similar series of runs were made, yielding the phase shift and amplitude attenuation for a lower speed of revolution. Also two runs, at points having both vertical and horizontal displacement, were made to obtain a general picture of the neutron waves thruout the subcritical assembly.

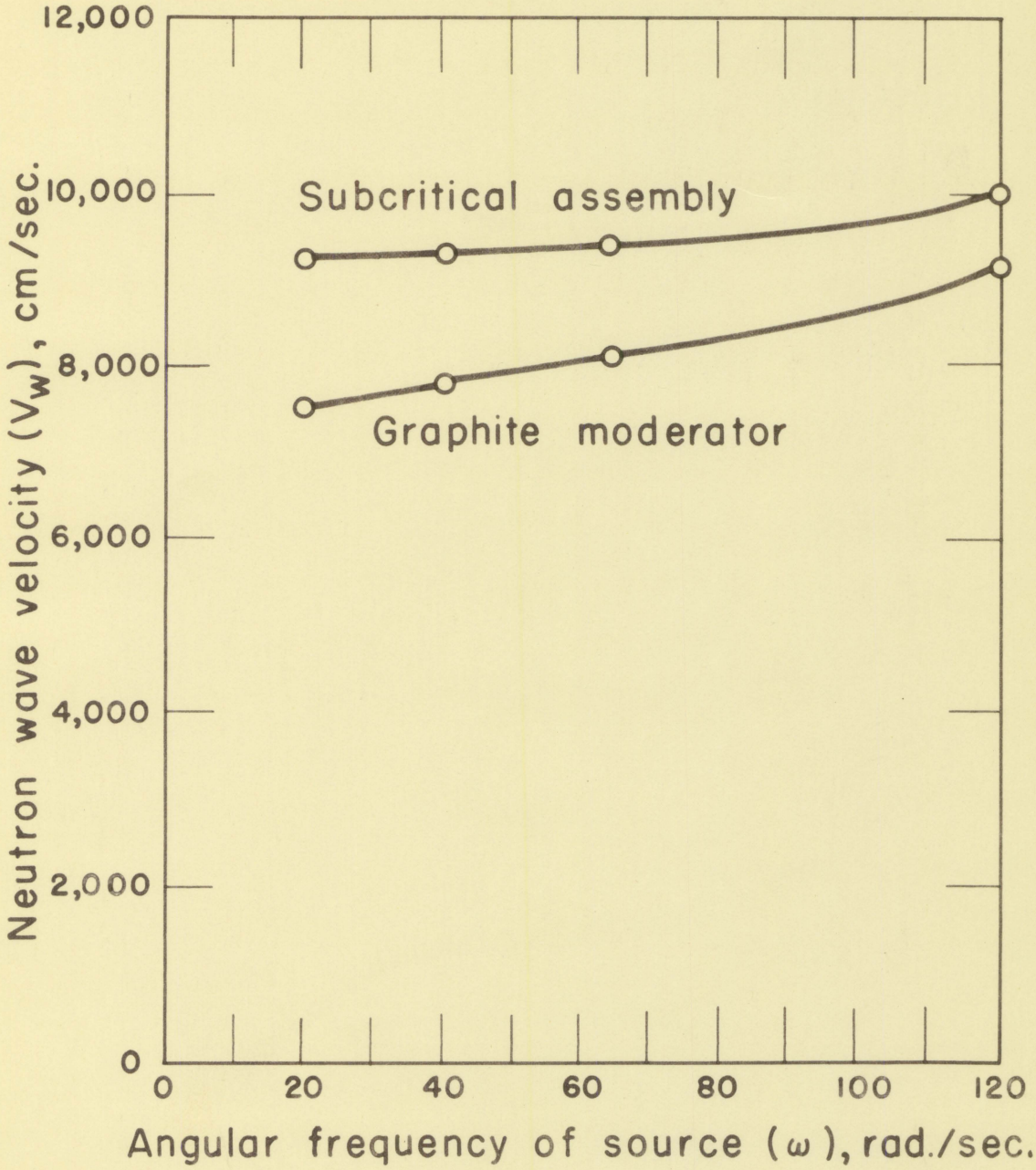

Fig. 5. Calculated wave velocity of the neutron wave

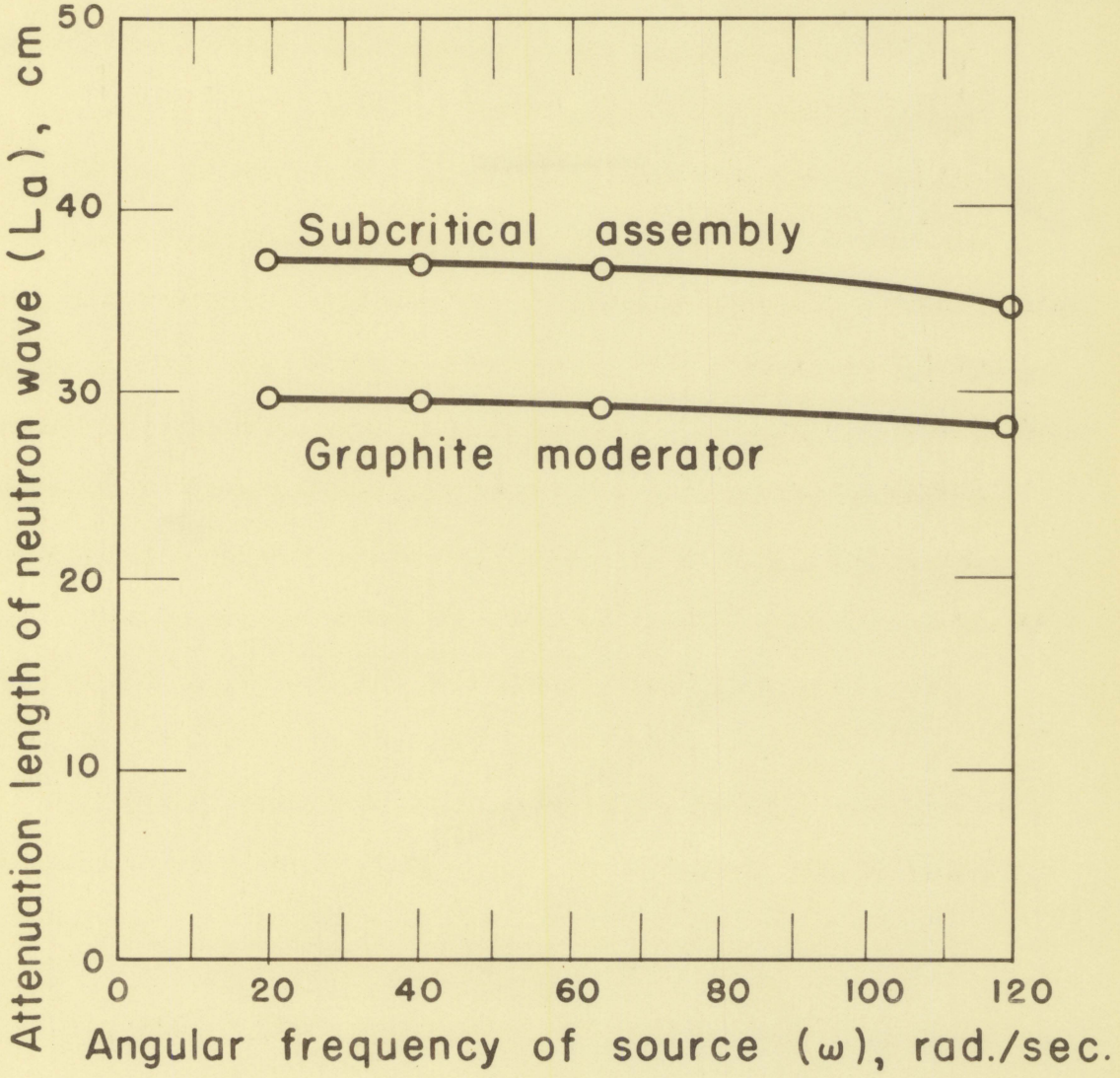

Fig. 6. Calculated attenuation length of the neutron wave

The original data for all runs completed are given in Tables 2 through 4 in the appendix. Both the phase angle shift with position and the attenuation length of the neutron wave were determined in this investigation, and the results were compared with those predicted from the theoretical consideration of the propagation of neutron waves in this particular subcritical assembly and in a graphite assembly.

The theory predicted a variation in both attenuation length and phase angle with increasing frequency of source oscillation. The propagation velocity increases with increasing frequency of oscillation, indicating that the medium is dispersive. The attenuation length decreases slightly with increasing frequency. The variation with angular frequency of these neutron wave properties for both the subcritical assembly and a graphite moderator is plotted in Fig. 5 and 6. The curves were calculated using Eq. (34), (35), (49) and (50) and the best value of the static material buckling previously determined (4), 51.6×10^{-6} cm.$^{-2}$.

The neutron wave propagation velocity is directly related to the variation in phase angle of the wave with distance. The relationship is given by

$$(71) \quad \frac{\text{Deg. of phase angle shift}}{\text{Inch}} = \frac{(\text{r.p.m.})(2.54)(360)}{V_w 60}$$

where the wave velocity V_w is given in cm./sec. This variation of phase angle of the neutron wave was the quantity which was

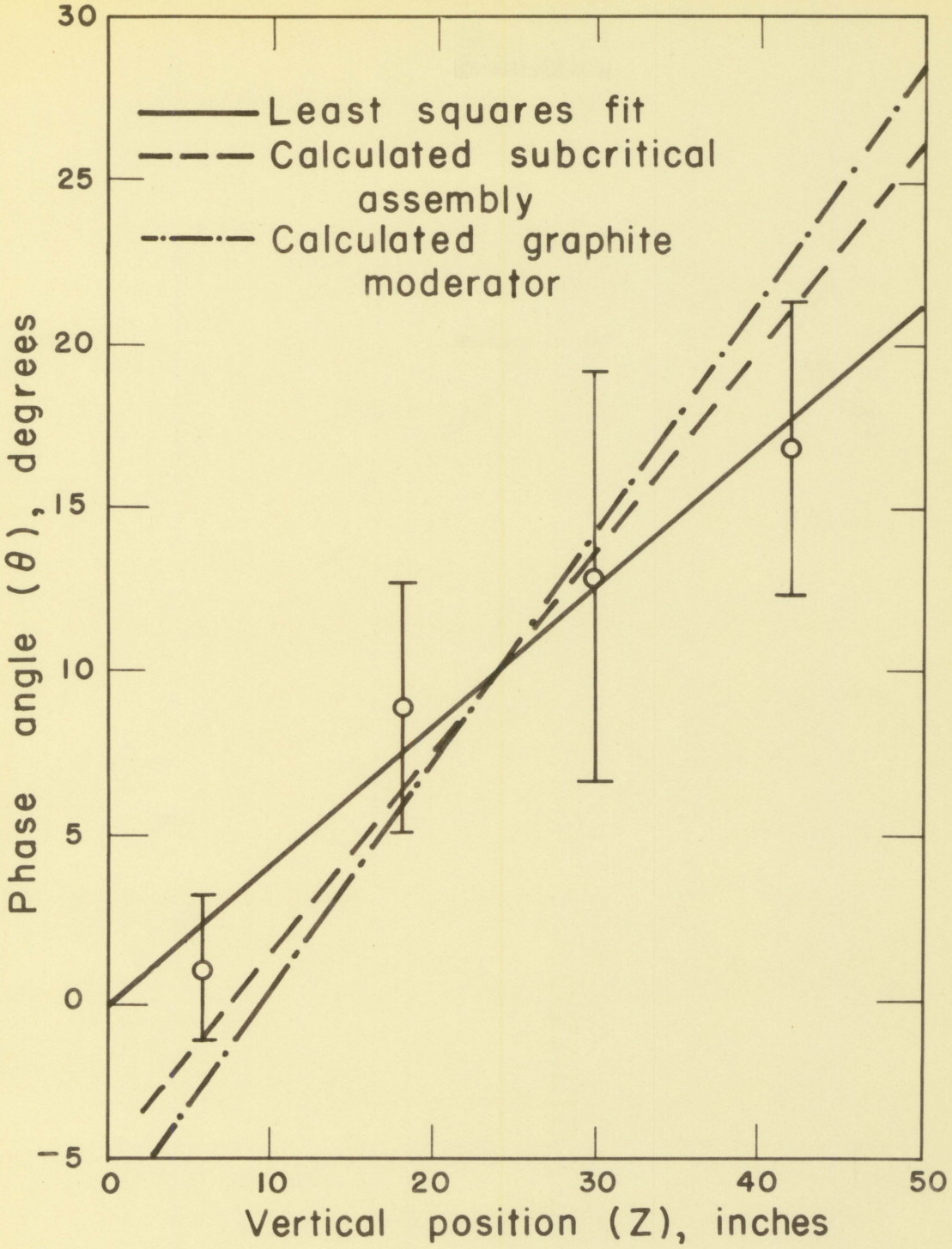

Fig. 7. Phase angle variation with vertical position for 380 r.p.m.

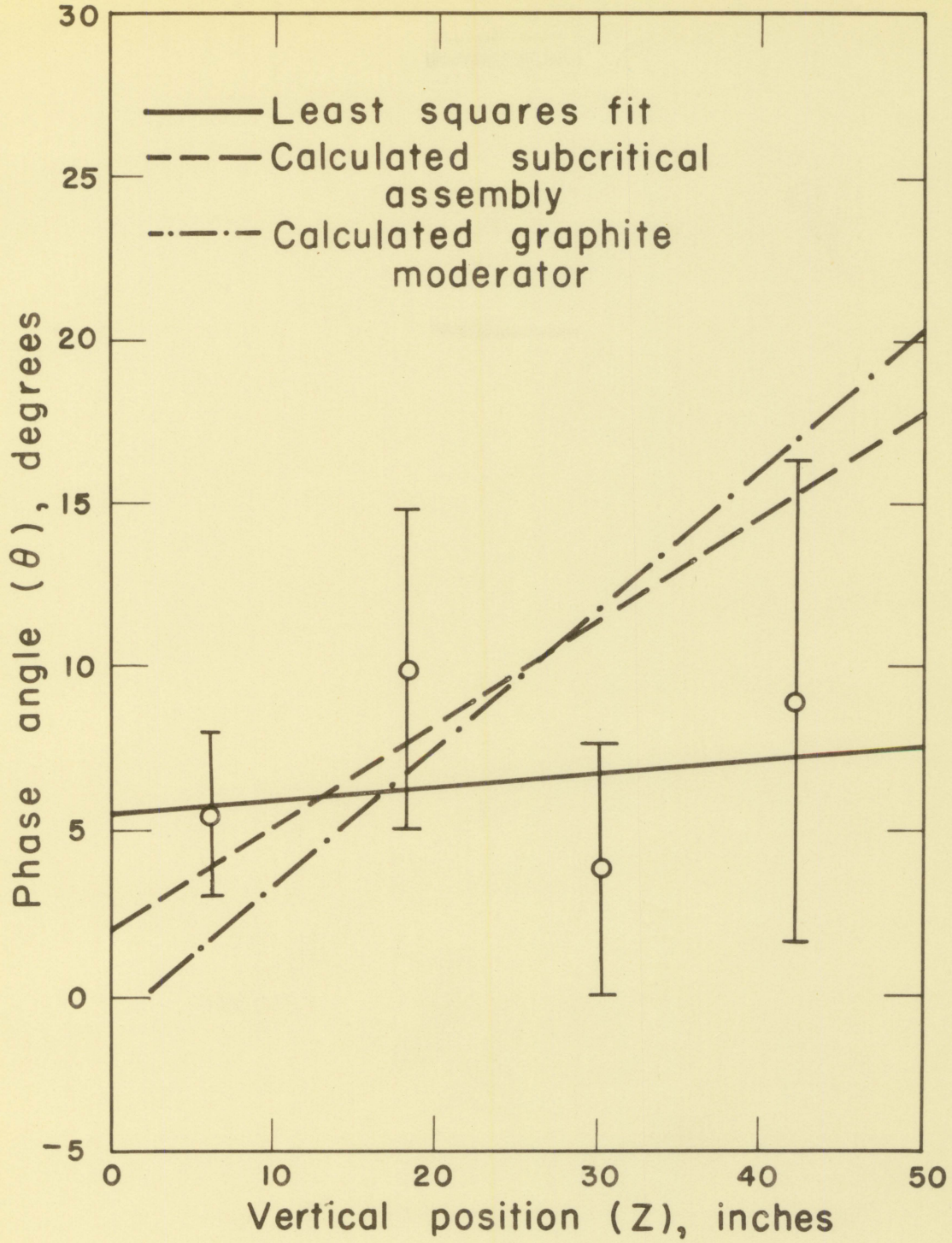

Fig. 8. Phase angle variation with vertical position for 190 r.p.m.

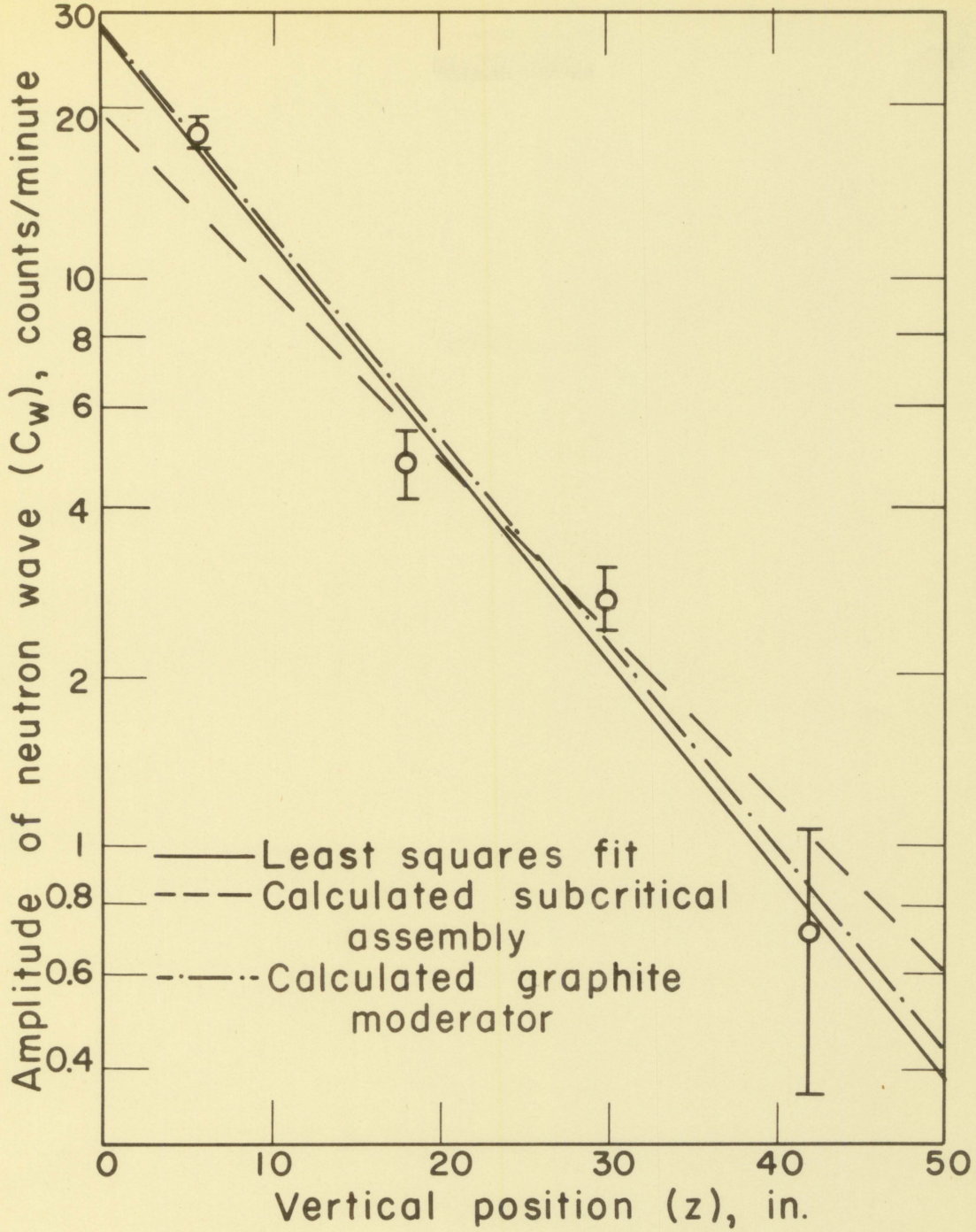

Fig. 9. Amplitude attenuation with vertical position for 190 r.p.m.

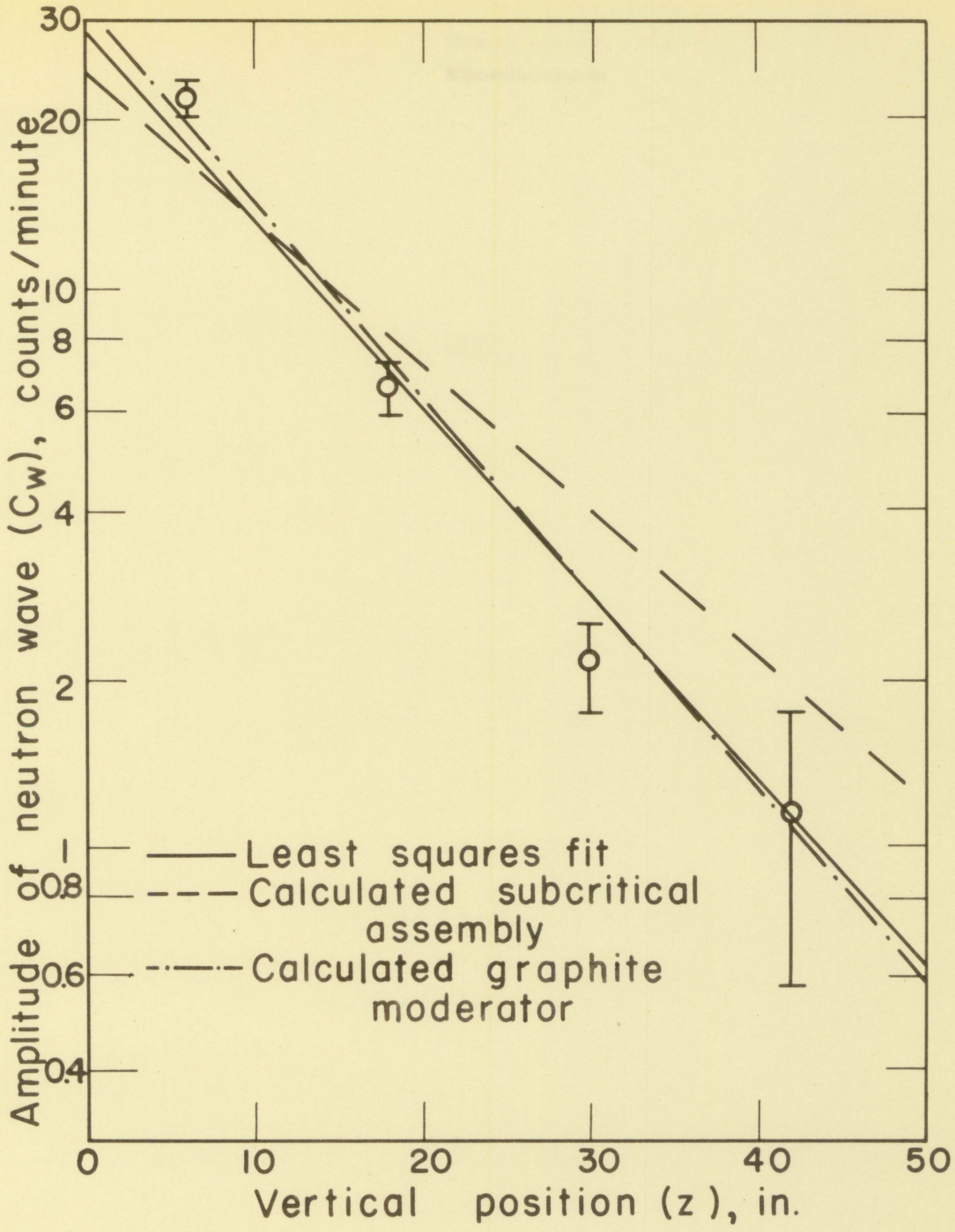

Fig. 10. Amplitude attenuation with vertical position for 380 r.p.m.

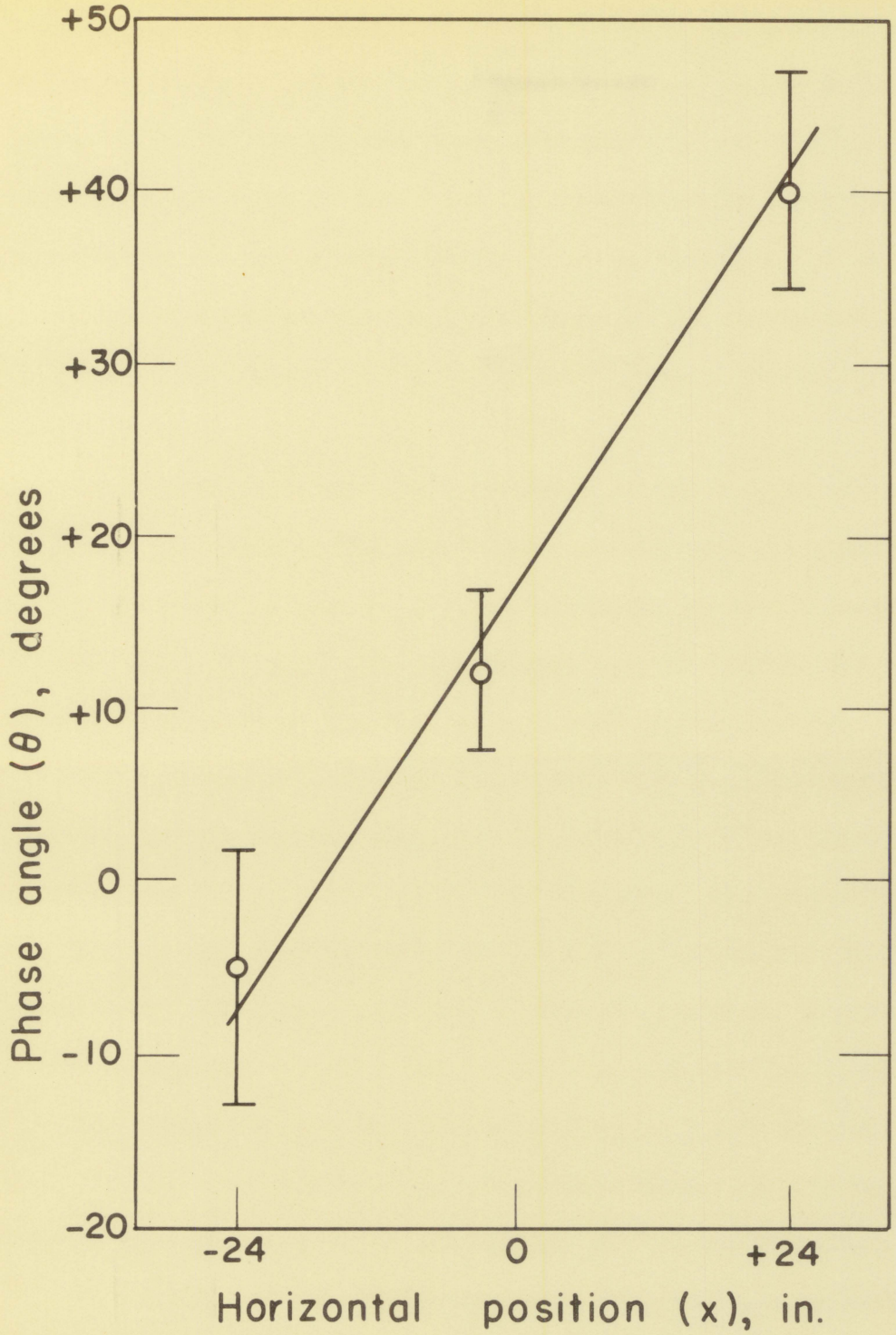

Fig. 11. Phase angle shift with horizontal position at the 24-in. level

experimentally determined. The values of the phase angle at various vertical positions for the two frequencies studied are shown in Fig. 7 and 8. The line through the points was drawn by use of the least-square fit. From the slope of this line the experimentally determined value of the neutron wave propagation velocity can be calculated by Eq. (50). The calculated values were 13,300 cm./sec. at 380 r.p.m. and 83,300 cm./sec. at 190 r.p.m. The value at 190 r.p.m. is considered to be erroneous.

Lines indicating the slope predicted by the theoretical considerations for the cases of the subcritical assembly and the graphite assembly are drawn in both Fig. 7 and 8. As can be seen the agreement between these lines and the experimental data is good in view of the standard deviation of the data as indicated in the figures.

The attenuation length of the neutron wave can be determined by plotting for the various positions the logarithm of any quantity proportional to the amplitude versus the position. The attenuation length can then be read directly from the graph. In Fig. 9 and 10, the experimentally determined amplitude at various positions is plotted, and a line through the points given by the least squares fit is shown.

The slopes for the two lines predicted by theory were obtained from Fig. 6. The experimentally determined values for the attenuation lengths were 32.0 cm. at 380 r.p.m. and 29.5 cm. at 190 r.p.m.

To give an overall qualitative description of the neutron wave propagation, determination of the phase and amplitude of the wave were made at points on the 24-in. level having both horizontal and vertical displacements from the oscillation source. Fig. 11 shows the lag of the

neutron wave in the horizontal direction. Again the best straight line was drawn through the points since the lead and lag of the wave relative to the center of the assembly should be equal from a consideration of symmetry.

VIII. DISCUSSION OF RESULTS

The behavior of the neutron waves studied agree qualitatively and semi-quantitatively with the behavior predicted by theoretical considerations of the propagation of an attenuated neutron wave in a subcritical assembly. In all cases the changes in the phase angle and amplitude were in the direction predicted by theory. Where the magnitude of those changes is not in complete agreement with theory the agreement is not unreasonable in view of the statistical deviations of the data. The various runs will be considered separately with comments appropriate to each one.

Fig. 5 and 6 show the behavior of the neutron wave as predicted by theory. It can be noted that at frequencies employed in this study, 19.8 and 39.6 radians per second, the neutron wave velocities and attenuation lengths change only slightly. The basis for this similarity is that at these frequencies the absolute value of the complex material buckling has not changed appreciably from the static material buckling. The change in the complex material buckling with frequency is much more pronounced at higher frequencies, as can be noted in Fig. 5 and 6.

Fig. 7 shows the variation of phase angle with vertical position at 380 r.p.m. while the slope of the line through the points is somewhat less than that expected by theory consideration of the standard deviation shown on the graph makes it apparent that withing the accuracy of the measurement the two slopes do not disagree.

Fig. 8 indicates the variation of phase angle with vertical position

at 190 r.p.m. The agreement here is poorer than at 380 r.p.m. While the theoretical velocities of propagation of the neutron waves are approximately equal at the two frequencies, Eq. (71) indicates that the phase angle shifts are different by a factor of almost two.

The variation of phase angle with position is less at the lower test velocity where the shift is so slight that it is masked by the statistical variation of the data. In view of the agreement shown in Fig. 7 the phase angle predictions seem reasonably valid for this system.

The attenuation lengths are shown in Fig. 9 and 10 and the agreement of the data with predicted values is approximately the same in both cases. The predicted attenuation lengths at the two frequencies are 37.1 and 36.7 cm. The two experimentally determined attenuation lengths were 32.0 and 29.5 cm., significantly lower than predicted. With the variation of the data taken, it is impossible to indicate whether this lower value of the attenuation length is valid.

Fig. 11 indicates the lag in phase angle detected by a horizontal traverse of the assembly at the 24-inch level performed at 380 r.p.m. Due to the arrangement of the assembly it was not possible to determine the phase angle directly at the desired center horizontal location and the value of the phase angle at the center was taken from Fig. 7. The neutron wave measured in the south channel definitely led and the neutron wave measured in the north channel lagged the oscillator in phase relative to the center channel. This is in agreement with the clockwise rotation of the oscillator drum as viewed from the east face. The straight line in the figure should not be taken as an indication of the

phase angle between these points of measurement. It merely indicates that the phase angle lag relative to the center of the assembly is equal to the phase angle lead which would be expected from the symmetry of the assembly.

In all cases the statistical variation is considerably larger than desirable, being caused by the combination of low count rates and the large steady state (C_s) component of the neutron wave.

The count rate was limited by the size of the neutron source and the sensitivity of the neutron detector. An increase in the length of time of counting was utilized by counting up to 2 hours in Channel 4. It was felt that any further extension of this time, beside entailing effort not commensurate with the slight statistical improvement, might also lead to other variations due to determinate errors such as temperature variation and moisture changes. The data in the appendix show clearly the fact that very small differences between very large numbers were taken. No suitable solution other than the reduction of steady-state count-rate seems possible.

The use of a very rapidly oscillating source can increase the absolute value of the complex material buckling material. The frequencies used in this study did not cause a large change in the absolute value of complex material buckling relative to the static material buckling.

An attempt was made to calculate the value of the static material buckling from Eq. (49) and Eq. (50) using the experimentally determined velocities and attenuation lengths. Results are shown in Table 1.

Table 1. Static material buckling

Revolutions per minute	Quantity measured	Static material buckling
380	Propagation velocity	-7.18×10^{-4}
380	Attenuation length	-1.97×10^{-4}
190	Propagation velocity	-5.98×10^{-2}
190	Attenuation length	-2.40×10^{-4}

However higher speeds of oscillation than were used can give a larger increase in the absolute value of the complex material buckling. The static material buckling is readily obtainable from the complex material buckling by Eq. (41). Hence values of the static material buckling comparable in precision to those obtained in a much larger subcritical assembly could be obtained.

IX. CONCLUSIONS

A theoretical and experimental investigation of the characteristics of the Iowa State University of Science and Technology graphite-uranium subcritical assembly by means of neutron waves was undertaken. From the phase and amplitude variation of the neutron wave, the velocity and attenuation lengths were determined permitting calculation of the complex and static material buckling. A method of analyzing the neutron wave through count rate determination was developed. Conclusions drawn were as follows.

1. The use of a periodically varying source definitely produced an attenuated neutron wave within the subcritical assembly.
2. In all cases studied the neutron wave changes were in the directions predicted by the theoretical developments.
3. The measured attenuation lengths of 32.0 and 29.5 cm. were lower than previous static measurements and also somewhat lower than predicted by theoretical considerations.
4. Measurements of neutron wave velocities by phase angle shifts requires higher frequencies of oscillation than were available with the existing equipment. The determination of a wave velocity of 13,300 cm./sec. at the higher of the two frequencies can be compared with the 9,260 cm./sec. predicted by the theory.
5. While the phase angle changes and attenuation of the amplitude agree within experimental error with those predicted theoretically, the precision of the experimental measurements

does not permit an accurate value of the static or complex material buckling to be calculated.

X. SUGGESTIONS FOR FURTHER STUDY

With the development of an experimental method of studying neutrons waves, several future studies could be suggested.

Higher frequencies of oscillation are desirable for any further study in order to obtain a better determination of the phase angle shift. At high frequencies the value of the complex material buckling would be significantly increased. In any case, the chain link drive probably should be eliminated for any high speed run.

As had been mentioned previously the large steady state component of the source greatly decreases the precision of the measurements. A re-design of the oscillator drum to eliminate most of the steady state components is necessary.

The performance of the electronic switching device was quite satisfactory and would seem to be capable of further use with no major changes. The rather obvious suggestions of use of stronger sources and more sensitive detectors should not however be overlooked.

XI. LITERATURE CITED

1. Campbell, E. C. and Stelson, P. H. Relaxation times of subcritical reactor by pulsed neutron techniques. Bulletin American Physical Society. 1: 183. 1956.

2. Glasstone, S. and Edlund, M. C. The elements on nuclear reactor theory. Princeton, N. J., D. Van Nostrand Co., Inc. 1952.

3. Raievski, V. and Horowitz, J. Mesure du libre parcours moyen de transport des neutrons thermiques dans l'ean lourde au moyen d'une source modules. Comptes Rendus. 238: 1993. 1954.

4. Uhrig, R. E. Transactions of the American Nuclear Society. 2: 1. 1959.

5. Weinberg, A. M. and Schweinler, H. C. Theory of oscillating absorber in a chain reactor. Physical Review 74: 851. 1948.

6. _____ and Wigner, E. P. The physical theory of neutron chain reactors. Chicago, Ill. The University of Chicago Press. 1958.

7. Worthington, A. C. and Geffner, J. Treatment of experimental data. New York, N. Y., John Wiley and Sons, Inc. 1955.

XII. ACKNOWLEDGMENTS

The author wishes to thank Dr. Robert E. Uhrig for his original suggestion of the problem studied in this thesis and for his many contributions which have been embodied in it. Without his unfailing optimism in the face of experimental difficulties and his generous donation of both time and effort this thesis would not now be complete.

The constant interest and wise direction of Dr. Murphy throughout this past year has proved invaluable and is gratefully acknowledged.

This thesis together with the course work of the past year has been completed under a fellowship granted by the Atomic Energy Commission. Their financial support, which has made possible full time academic work without monetary distractions, has been deeply appreciated.

XIII. APPENDIX

Table 2. Data at 380 r.p.m.

Channel	Interval 1		Interval 2	
	RIDL C/7.5 Min.	N - C C/15 Min.	RIDL C/7.5 Min.	N - C C/15 Min.
1	448457	896195	464633	885351
2	219206	436568	227858	441055
2	221837	441621	226391	442277
3	99822	198745	100505	197067
3	99304	197183	102089	199343
3	99391	198293	100694	197789
4	42762	84770	44461	86539
4	42670	84396	44288	86103
4	42839	84974		
4	42395	84274		
4	42128	83393		
4	42679	83876		
4	42710	84563		
4	42553	84161		
North	97106	190173	98213	191655
South	86885	174347	90463	175134

Table 3. Data at 190 r.p.m.

	Interval 1		Interval 2	
Channel	RIDL C/7.5 Min.	N - C C/15 Min.	RIDL C/7.5 Min.	N - C C/15 Min.
1	436292	869188	457743	879505
2	215835	430291	221419	432782
2	216625	431385	220098	431202
3	97266	193759	101580	193668
3	97113	193938	99080	194315
3	96678	193289	99470	194320
3	96723	193133	98786	193373
4	41840	83559	42570	83252
4	42450	84031	42259	83339
4	42005	83820	42624	83813
4	42322	84089	42579	84100
4	42678	85222		
4	41309	83652		
4	42971	85192		
4	41813	83493		

Table 4. Phase angle and amplitude in various channels

Channel	380 r.p.m.		190 r.p.m.	
	θ	C_w	θ	C_w
1	0.93 ± 2.15	21.7 ± 0.825	5.39 ± 2.53	18.2 ± 0.450
2	8.78 ± 3.70	6.35 ± 0.590	9.93 ± 4.76	4.72 ± 0.588
3	12.82 ± 6.30	2.11 ± 0.400	3.73 ± 3.96	2.78 ± 0.388
4	16.82 ± 4.45	1.27 ± 0.500	8.76 ± 7.30	0.70 ± 0.350
North	+ 40.23 ± 6.88			
South	- 5.68 ± 7.22			